Detailed photoluminescence study of $Cu_2Ge(SSe)_3$ microcrystals

Cite as: AIP Advances 11, 085105 (2021); doi: 10.1063/5.0053928
Submitted: 15 April 2021 • Accepted: 22 July 2021 •
Published Online: 3 August 2021

J. Krustok,[1,2,a] R. Kaupmees,[2] X. Li,[2] M. Kauk-Kuusik,[2] and M. Grossberg[2]

AFFILIATIONS

[1] Division of Physics, Tallinn University of Technology, Ehitajate Tee 5, 19086 Tallinn, Estonia
[2] Department of Materials and Environmental Technology, Tallinn University of Technology, Ehitajate Tee 5, 19086 Tallinn, Estonia

[a] **Author to whom correspondence should be addressed:** juri.krustok@taltech.ee

ABSTRACT

We present a detailed temperature and laser power dependent photoluminescence (PL) study of $Cu_2Ge(S_{0.4}Se_{0.6})_3$ microcrystals. At $T = 20$ K, two relatively narrow PL peaks were detected at about 1.16 eV (peak No. 1) and 1.12 eV (peak No. 2) and a weak, broad PL band was detected at about 0.82 eV (peak No. 3). The temperature and laser power dependencies indicate that at $T = 20$ K, the properties of PL peak Nos. 1 and 2 can be explained by the distant donor–acceptor (DA) pair model where a donor defect has a depth of $E_D \approx 20$ meV and $E_D \approx 60$ meV for peak Nos. 1 and 2, respectively. The depth of acceptor defects was 57 and 76 meV for peak Nos. 1 and 2, respectively. At around $T = 90$ K, the DA pair recombination of peak No. 1 gradually starts to transform into the conduction band–acceptor recombination, but peak No. 2 shows a DA pair recombination even at room temperature. The estimated bandgap energy of this compound at room temperature was $E_g = 1.225$ eV.

I_2–IV–VI_3 compounds Cu_2MS_3 (M = Sn and Ge) have recently received increasing attention as candidates for the absorber layer of thin-film solar cells. Among them, Cu_2GeS_3 (CGS) and Cu_2GeSe_3 have direct bandgap energies of 1.65 and 0.82 eV, respectively.[1–3] Unfortunately, the bandgap energy of both compounds is far from ideal for single junction solar cells, and therefore, solid solutions $Cu_2Sn_{1-x}Ge_xS_3$ have been used in order to reduce the bandgap energy of CGS. The record efficiency of these solar cells is 6.73%.[4] The cation substitution mainly affects the position of the conduction band edge. An alternative approach involves substitution of S by Se and thus shifting the energy of the valence band edge in $Cu_2Ge(S_xSe_{1-x})_3$ (CGSSe) solid solutions. Unfortunately, there is very little information about properties of CGSSe solid solutions and there are no attempts to prepare solar cells using these solid solutions. A recent study of CGSSe nanocrystals showed that there is nearly linear relationship between the bandgap energy and the Se content in the CGSSe solid solutions, and thereby, it is possible to tune the bandgap energy to the ideal range for solar light absorption.[5] However, the defect structure of CGSSe is still not studied, while the properties of Cu_2GeS_3 and Cu_2GeSe_3 compounds are more or less known. The photoluminescence spectroscopy (PL) has been a main tool to study defects in many compounds. Therefore, in this paper, we will present a first and detailed PL study of $Cu_2Ge(S_xSe_{1-x})_3$ microcrystals, where x = 0.4.

$Cu_2Ge(S_{0.4}Se_{0.6})_3$ microcrystalline powder was synthesized by the molten salt method. 5N purity Cu, Ge, S, and Se were used as precursors and LiI as a reaction medium. All chemicals with a chemical composition of 33.32 mol. % Cu, 16.67 mol. % Ge, 19.97 mol. % S, and 30.03 mol. % Se corresponding to the formula $Cu_2Ge(S_{0.4}Se_{0.6})_3$ were mixed and ground in an agate mortar. These operations were carried out in a glove box under an argon atmosphere. The mixture was put into the carbon coated quartz ampoule and sealed under a vacuum of 3×10^{-2} Torr. The powder synthesis was carried out at 700 °C in a closed quartz ampoule. The heating rate was maintained at 0.5 °C/min up to the requisite synthesis temperature and held for 100 h. Finally, the obtained product was cooled to room temperature in air and then washed with deionized water to release the powder crystals from the LiI salt. Before PL measurements, the powder crystal surfaces were cleaned from residues chemically with 1 wt. % Br-MeOH solution followed by 10 wt. % KCN and

isothermally annealed at 300 °C for 35 min. The shape and surface morphology of the synthesized microcrystals were studied with a high-resolution scanning electron microscope (SEM), Zeiss MERLIN. The average size of our microcrystals was around 80 μm; see Fig. 1(a).

The elemental composition of microcrystals was determined by Energy Dispersive X-ray (EDX) spectroscopy. Bulk composition of micro-crystalline powder was measured from polished crystals. According to EDX results, the average composition of synthesized microcrystals was $Cu_{2.01}Ge_{0.99}(S_{0.4}Se_{0.6})_3$.

The crystal structure of the studied $Cu_2Ge(S_{0.4}Se_{0.6})_3$ microcrystals was determined by x-ray diffraction (XRD) using a Rigaku Ultima IV diffractometer operating with the silicon strip detector D/teX Ultra. XRD analysis showed an orthorhombic crystal structure with the space group *Imm*2. No other phases were detected. Unfortunately, there are no XRD data for the $Cu_2Ge(S_{0.4}Se_{0.6})_3$ compound, but the closest match is the $Cu_2Ge(S_{0.2}Se_{0.8})_3$ compound (ICDD PDF-2-2013, 00-059-0291). Figure 1(b) shows that due to different S/Se ratios in our crystals, all XRD peaks are slightly shifted toward higher angle values, but the overall coincidence is quite good. The lattice constants were determined using the Rietveld refinement procedure by Rigaku PDXL version 1.4.0.3 software. The obtained lattice parameters were a = 11.626 Å, b = 3.883 Å, and c = 5.376 Å. We also expect that a small amount of Li is present in our crystals, and therefore, it could have a slight effect on lattice constants of our microcrystals.

Raman measurements were carried out using a Horiba LabRAM HR800 micro-Raman system equipped with a cooled multichannel CCD detection system in the backscattering configuration with a spectral resolution better than 1 cm^{-1}. A YAG:Nd laser (wavelength λ = 532 nm) was used for excitation. The laser spot size was about 2 μm in diameter. Figure 1(c) presents the deconvoluted Raman spectra of $Cu_2Ge(S_{0.4}Se_{0.6})_3$ microcrystals fitted using a Lorentzian function to resolve the peaks. As with all solid solutions, the Raman spectrum includes the contribution of both sulfide and selenide. The most intense Raman peaks in Cu_2GeSe_3 are at 189 and 266 cm^{-1},[6] while in Cu_2GeS_3, similar peaks can be found at 339 and 396 cm^{-1}.[1,7,8] In solid solutions, all sulfide related peaks tend to shift toward smaller wavenumbers and the relative intensity of these peaks decreases and selenide related peaks will shift toward higher wavenumbers and their intensity decreases. Almost all Raman modes of solid solutions follow the two-mode behavior as in other sulfide–selenide solid solutions and become wider.[9,10] In our solid solution, the selenide related peaks dominate at around 200 cm^{-1} and sulfide related peaks around 380 cm^{-1} are quite weak. All detected Raman peaks belong to our solid solution, and no other phases are present.

A 0.64 m focal length single grating (600 mm^{-1}) monochromator and the 442 nm line of a He–Cd laser with different powers were used for PL measurements. For PL signal detection, a Hamamatsu InGaAs photomultiplier tube (PMT) was used. A closed-cycle helium cryostat was employed to measure temperature dependencies of the PL spectra at temperatures from 20 to 300 K. The laser spot size for these measurements was 200 μm in diameter.

The low temperature PL spectrum of CGSSe shows three bands, No. 1 at 1.16 eV, No. 2 at 1.12 eV, and a wide and weak No. 3 band at 0.82 eV; see Fig. 2(a). Unfortunately, this band was too weak for further analysis, but the presence of this rather deep band proves that quite deep defect levels are also present in CGSSe. Band Nos. 1 and 2 were fitted using an asymmetric double sigmoidal fitting function because both bands had slightly asymmetric shape; see Fig. 2(b). The full-width at half-maximum (FWHM) of band No. 1 was around 30 meV, while band No. 2 was significantly wider with a FWHM of ≈ 55 meV. A very similar double band arrangement of low temperature PL spectra was discovered also in CGS[1] and in CGSe.[2] On increasing the temperature, both bands show a small shift toward higher energy and a drastic change in shape at T = 40–90 K; see Fig. 2(a). This blueshift at a low temperature is typical for donor–acceptor (DA) pairs where the low temperature DA emission is replaced by conduction band–acceptor (c–A) recombination due to ionization of shallow donor levels of the DA pair.[11–13] However, band No. 2 seems to be less affected. Therefore, it is possible that band No. 2 is related to deeper donor (and acceptor) levels and the DA recombination is not changed to c–A recombination in the measured temperature range, but we only observe a redistribution of recombination from closer DA pairs to more distant ones. At T = 40–80 K, the FWHM of peak No. 1 shows an abrupt increase indicating the presence of both DA pair and c–A PL peaks; see Fig. 3(a).

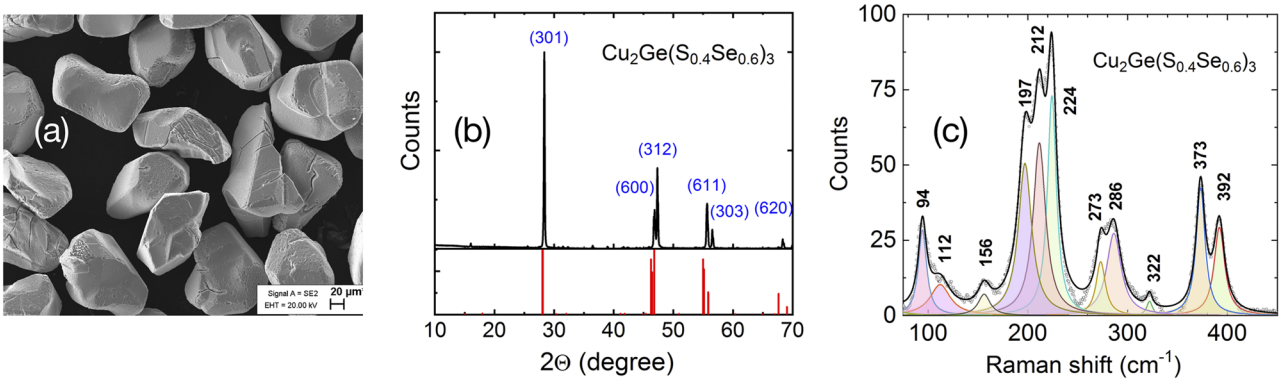

FIG. 1. (a) SEM image of CGSSe microcrystals. (b) Measured XRD pattern of $Cu_2Ge(S_{0.4}Se_{0.6})_3$ microcrystals and a theoretical pattern of the $Cu_2Ge(S_{0.2}Se_{0.8})_3$ compound (ICDD PDF-2-2013, 00-059-0291) (red lines). (c) Raman spectra of the CGSSe solid solution together with fitting results using a Lorentzian line shape.

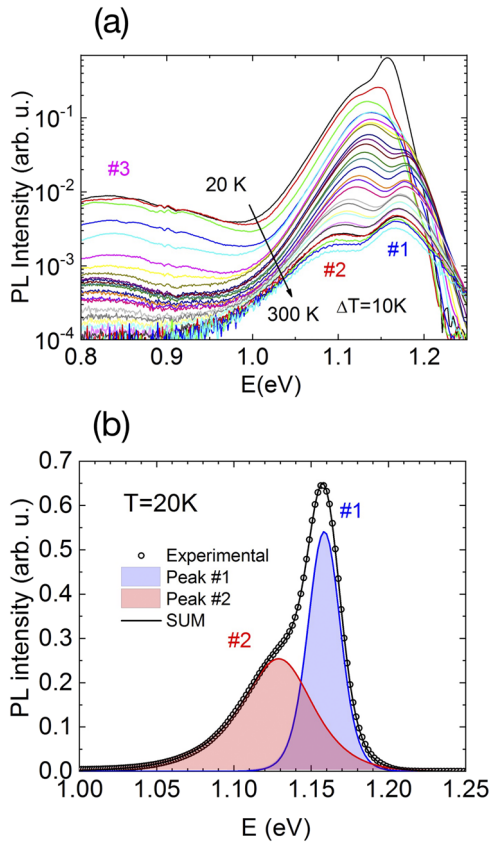

FIG. 2. (a) Temperature dependence of the PL spectrum and (b) example of PL fitting using an asymmetric double sigmoidal function at T = 20 K.

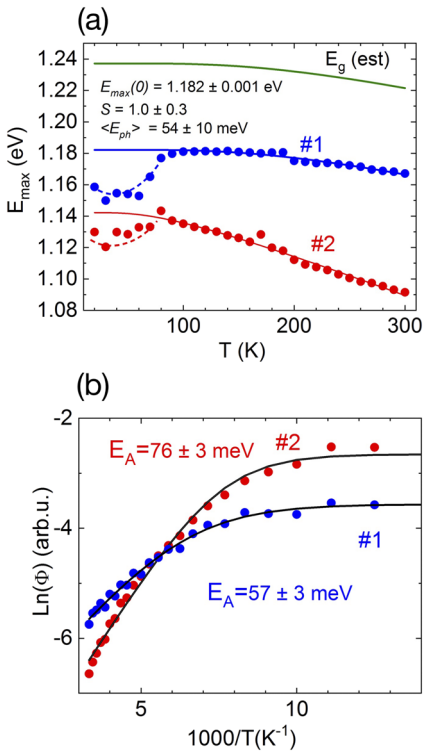

FIG. 3. (a) Temperature dependence of peak positions for peak Nos. 1 and 2 together with an estimated value of E_g. Fitting of peak No. 1 using Eq. (1) is given as a blue line; fitting parameters are given. The red line for peak No. 2 is a guide to the eye. (b) Arrhenius plot of integral intensity for both peaks together with the fitting result obtained using Eq. (3).

The temperature dependence of the peak position obtained from the fittings of the PL spectra is plotted in Fig. 3(a). Experimental data points of peak No. 1 at T = 100–300 K were fitted with O'Donnell's expression[14]

$$E_{max}(T) = E_{max}(0) - S\langle E_{ph}\rangle\left[\coth\left(\langle E_{ph}\rangle/2kT\right) - 1\right], \quad (1)$$

where $E_{max}(0)$ is the peak position at T = 0 K, S is a dimensionless coupling constant, and $\langle E_{ph}\rangle$ represents an average phonon energy. The obtained phonon energy of 54 meV corresponds to 436 cm^{-1}, and it is located at slightly higher energy than the highest detected Raman modes. All parameters of this fitting are given in Fig. 3(a). Assuming that peak No. 1 at this temperature range is related to c–A recombination and the peak shift with temperature is explained by the temperature dependence of E_g, we can estimate also the temperature dependence of E_g if we know the depth of the acceptor level. Peak No. 2 however shows more rapid shift with increasing temperature. It is known that the PL peak energy for every single DA pair recombination is expressed as

$$E_i(r) = E_g - (E_D + E_A) + \frac{e^2}{\varepsilon r_i}, \quad (2)$$

where E_g, E_D, and E_A are the bandgap energy and the donor and acceptor ionization energies, respectively; r_i is the distance between the donor and acceptor defects; and ε is the static dielectric constant.[15] This means that the FWHM of peak No. 2 is wider because of wider distribution of DA pair distances. At higher temperatures, defects from the closest DA pairs will be ionized and the distribution will shift toward more distant pairs having smaller peak position energy. Therefore, the peak position shift of peak No. 2 is a combined effect of the DA pair distribution shift and the E_g shift.

The thermal activation energies for the bands obtained from the Arrhenius plot [Fig. 3(b)] where the dependence of $\ln\Phi$ (T) vs 1000/T was fitted by using a theoretical expression for discrete energy levels,[16]

$$\Phi(T) = \Phi_0 \Big/ \left[1 + A_1 T^{3/2} + A_2 T^{3/2} \exp(-E_A/kT)\right], \quad (3)$$

where Φ is the integrated intensity of the PL band, A_1 and A_2 are the process rate parameters, and E_A is the thermal activation energy. Fitting results are presented in Fig. 3(b). The thermal activation energy of peak No. 1 represents the depth of the acceptor level E_A = 57 ± 3 meV. By using this acceptor defect depth value, we were able to estimate the temperature dependence of E_g; see Fig. 3(a). The temperature dependence of the bandgap energy of CGSSe crystals is rather small, and a very small shift of E_g was also detected in CGS and

CGSe crystals.[1,2,17,18] As was predicted, the activation energy for peak No. 2 is higher and, consequently, peak No. 2 is related to deeper defects.

Next, the temperature dependence of the full-width at half-maximum was fitted using the relation proposed by Rudin and Reinecke[19] given as

$$\mathrm{FWHM(T)} = \mathrm{W_0} + \beta \mathrm{T} + \mathrm{W_1}/[\exp(\mathrm{E_{ph}}/\mathrm{kT}) - 1], \quad (4)$$

where W_0 is the width at $T = 0$ K also including inhomogeneous broadening, β is a coefficient for the interaction of excitons with acoustic phonons, the last term represents the interaction with optical phonons, and E_{ph} is the phonon energy. The interaction with acoustic phonons was neglected because it is usually very small. The fitting result is presented in Fig. 4(a) for both bands. Obtained phonon modes 16 and 24 meV correspond to Raman modes related to CGSe (129 and 194 cm^{-1}, respectively).

By increasing the laser power, the shape of the PL spectra did not show any dramatic changes, i.e., the integrated intensity Φ of all peaks increases almost linearly with laser power [see Fig. 4(b)] and the experimental data can be fitted by the simple power law of the form $\Phi \propto L^m$, where Φ is the PL integrated intensity, L is the excitation laser power, and m is a dimensionless exponent. It is well known that for an excitation laser photon with an energy exceeding the bandgap energy, the coefficient m is generally $1 < m < 2$ for the free- and bound-exciton emission and $m \leqq 1$ for free-to-bound and donor–acceptor pair recombinations.[20] Thus, the obtained value of $m \approx 1$ for both bands is a sign that all measured PL bands are related to defects and do not have an excitonic nature. At the same time, both PL bands show a certain blueshift with laser power; see the inset in Fig. 4(b). The blueshift is typical for donor–acceptor (DA) pairs with different distances between donor and acceptor defects in the crystal lattice.[21–23] The rate of this blueshift is usually higher for DA pairs with shorter distances. Accordingly, PL band Nos. 1 and 2 with a blueshift of 2 meV/decade of laser power must be related to quite shallow defects. We assume that all the donor and/or acceptor levels observed are native and due to deviations in composition from the ideal stoichiometry. The shallowest acceptor level with $E_A = 57$ meV is very close to the V_{Cu} level observed in CGSe crystals by PL and electrical measurements (about 50–65 meV).[2,24] Remarkably lower activation energies were measured in CGS crystals,[1] and it seems that sulfur has an effect of reducing the activation energy of acceptor defects. At the same time, the deeper acceptor level in CGSe crystals is believed to be related to the selenium interstitial defect with an activation energy of $E_A = 120$ meV.[24] Our measurements show

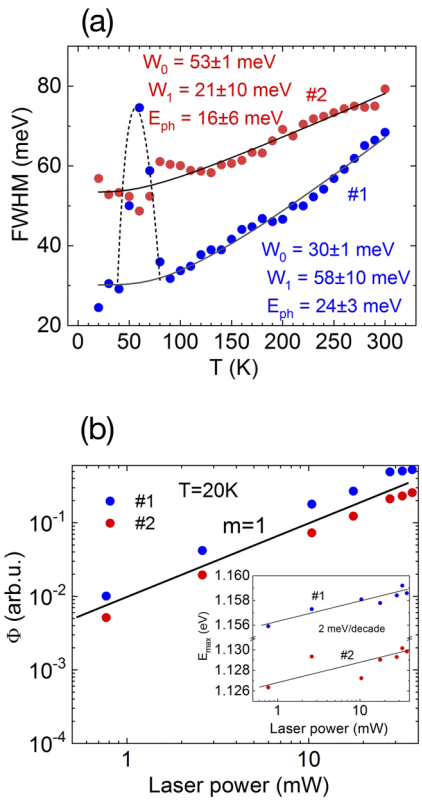

FIG. 4. (a) The temperature dependence of FWHM for both bands and fitting result (lines) and fitting parameters obtained using Eq. (4). (b) Laser power dependence of integral intensity for both bands; the inset shows the peak position shift with laser power.

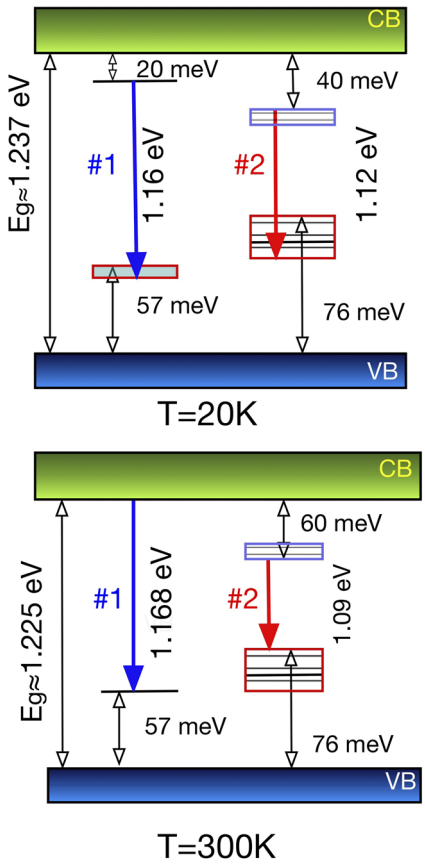

FIG. 5. Energy band diagram of the CGSSe solid solution, illustrating the recombination processes at $T = 20$ and at $T = 300$ K. Distribution of DA pair energy levels is shown as blue and red boxes.

an activation energy of E_A = 76 meV. This level can be related to the S/Se interstitial defect or to the antisite Cu_{Ge} defect.[2] We also have two shallow donor levels ($E_D \approx 20$ and 60 meV) in our sample. The most probable donor defect could be the Ge_{Cu} antisite defect, but the origin of donor defects is not clear at the moment and further studies are needed.

In conclusion, we present a recombination model for the $Cu_2Ge(S_{0.4}Se_{0.6})_3$ microcrystals; see Fig. 5. At low temperatures, the DA pair recombination is dominating for both PL peaks. At temperatures $T > 90$ K, the DA pair recombination is gradually transformed into c–A recombination for peak No. 1, but peak No. 2 shows a DA pair recombination even at room temperature. The distribution of DA pair energy levels for peak No. 2 is wider due to shorter distances between donor and acceptor defects. According to this model, the estimated bandgap energy E_g at room temperature is about 1.225 eV, and this value is very close to the bandgap energy of $Cu(In,Ga)Se_2$ absorbers in record breaking thin-film solar cells.[25]

This work was supported by the European Regional Development Fund (Project No. TK141) and by the Estonian Research Council (Project No. PRG1023). M.G. acknowledges the L'Oréal Baltic For Women in Science Program. Dr. V. Mikli is thanked for his help with EDX measurements.

DATA AVAILABILITY

The data that support the findings of this study are available from the corresponding author upon reasonable request.

REFERENCES

[1] N. Aihara, Y. Matsumoto, and K. Tanaka, Phys. Status Solidi **254**, 1700118 (2017).
[2] G. Marcano, G. S. Pérez, and C. Rincón, Phys. Status Solidi B **254**, 1700332 (2017).
[3] H. Araki, K. Chino, K. Kimura, N. Aihara, K. Jimbo, and H. Katagiri, Jpn. J. Appl. Phys., Part 1 **53**, 05FW10 (2014).
[4] M. Umehara, S. Tajima, Y. Aoki, Y. Takeda, and T. Motohiro, Appl. Phys. Express **9**, 072301 (2016).
[5] C. Yang, B. Zhou, S. Miao, C. Yang, B. Cai, W.-H. Zhang, and X. Xu, J. Am. Chem. Soc. **135**, 5958 (2013).
[6] G. Marcano, C. Rincón, G. Marín, G. E. Delgado, A. J. Mora, J. L. Herrera-Pérez, J. G. Mendoza-Alvarez, and P. Rodríguez, Solid State Commun. **146**, 65 (2008).
[7] Y. Matsumoto, N. Aihara, N. Saito, and K. Tanaka, Mater. Lett. **194**, 16 (2017).
[8] Y. Kim and I.-H. Choi, J. Alloys Compd. **770**, 959 (2019).
[9] M. Grossberg, J. Krustok, J. Raudoja, K. Timmo, M. Altosaar, and T. Raadik, Thin Solid Films **519**, 7403 (2011).
[10] R. Bacewicz, W. Gebicki, and J. Filipowicz, J. Phys.: Condens. Matter **6**, L777 (1994).
[11] L. Bai, N. C. Giles, P. G. Schunemann, T. M. Pollak, K. Nagashio, and R. S. Feigelson, J. Appl. Phys. **95**, 4840 (2004).
[12] M. V. Yakushev, I. Forbes, A. V. Mudryi, M. Grossberg, J. Krustok, N. S. Beattie, M. Moynihan, A. Rockett, and R. W. Martin, Thin Solid Films **582**, 154 (2015).
[13] J. Krustok, T. Raadik, R. Kaupmees, F. Ghisani, K. Timmo, M. Altosaar, V. Mikli, and M. Grossberg, J. Phys. D.: Appl. Phys. **54**, 105102 (2021).
[14] K. P. O'Donnell and X. Chen, Appl. Phys. Lett. **58**, 2924 (1991).
[15] D. G. Thomas, M. Gershenzon, and F. A. Trumbore, Phys. Rev. **133**, A269 (1964).
[16] J. Krustok, H. Collan, and K. Hjelt, J. Appl. Phys. **81**, 1442 (1997).
[17] B. K. Sarkar, A. S. Verma, and P. S. Deviprasad, Physica B **406**, 2847 (2011).
[18] G. Marcano and L. Nieves, J. Appl. Phys. **87**, 1284 (2000).
[19] S. Rudin and T. L. Reinecke, Phys. Rev. B **41**, 3017 (1990).
[20] T. Schmidt, K. Lischka, and W. Zulehner, Phys. Rev. B **45**, 8989 (1992).
[21] N. Aihara, K. Tanaka, H. Uchiki, A. Kanai, and H. Araki, Appl. Phys. Lett. **107**, 032101 (2015).
[22] C. Spindler, D. Regesch, and S. Siebentritt, Appl. Phys. Lett. **109**, 032105 (2016).
[23] N. Shrestha, C. R. Grice, E. Bastola, G. K. Liyanage, A. B. Phillips, M. J. Heben, Y. Yan, and R. J. Ellingson, MRS Adv. **3**, 3293 (2018).
[24] G. Marcano, D. B. Bracho, C. Rincón, G. S. Pérez, and L. Nieves, J. Appl. Phys. **88**, 822 (2000).
[25] L. M. Mansfield, R. L. Garris, K. D. Counts, J. R. Sites, C. P. Thompson, W. N. Shafarman, and K. Ramanathan, IEEE J. Photovoltaics **7**, 286 (2017).